Applied Physics Letters

RESEARCH ARTICLE | AUGUST 12 2024

Analysis on dual Fano resonance in a coupled-resonator waveguide

Zhiwei Wei ; Tingge Yuan ; Jiangwei Wu ; Chengyu Chen ; Yuping Chen ; Xianfeng Chen

Appl. Phys. Lett. 125, 073501 (2024)
https://doi.org/10.1063/5.0225699

Applied Physics Letters ARTICLE pubs.aip.org/aip/apl

Analysis on dual Fano resonance in a coupled-resonator waveguide

Cite as: Appl. Phys. Lett. **125**, 073501 (2024); doi: 10.1063/5.0225699
Submitted: 26 June 2024 · Accepted: 29 July 2024 ·
Published Online: 12 August 2024

View Online Export Citation CrossMark

Zhiwei Wei,[1] Tingge Yuan,[1] Jiangwei Wu,[1] Chengyu Chen,[1] Yuping Chen,[1,a)] and Xianfeng Chen[1,2]

AFFILIATIONS

[1]State Key Laboratory of Advanced Optical Communication Systems and Networks, School of Physics and Astronomy, Shanghai Jiao Tong University, Shanghai 200240, China
[2]Collaborative Innovation Center of Light Manipulations and Applications, Shandong Normal University, Jinan 250358, China

[a)]Author to whom correspondence should be addressed: ypchen@sjtu.edu.cn

ABSTRACT

Dual Fano resonance was demonstrated in a compact coupling system without additional large footprint tunable devices consisting of a grating-coupled waveguide and a micro-racetrack resonator on thin film lithium niobate. A multimode interference model was proposed for the dual Fano resonance system. The inverse design method was used to realize model fitting, validate our model, and analyze our model. Based on the parameters obtained by the inverse design, we further analyzed the influence of different parameters. Our research also shows that through the interaction of two Fano resonance modes, tunable line shape and enhanced extinction ratio can be realized in the transmission spectrum, which has potential applications in optical sensing.

Fano resonance originates from the interference between the discrete mode and the continuous mode.[1] Depending on the phase difference of the interference modes, the spectral line shapes of Fano resonance can change from the typical asymmetric shape to a Lorentz dip or electromagnetically induced transparency (EIT)-like peak.[2] Different photonic structures have been designed to realize Fano resonance, such as photonic crystals,[3] plasmonic nanostructure,[4] metamaterials,[5] and micro-resonators.[6–17] Among them, due to the high-quality factor and small mode volume of the whispering gallery mode resonator, the Fano resonance spectrum in the whispering gallery mode resonator was narrow and steep, which attracted lots of interest. To date, Fano resonance has been shown to have many potential applications, such as sensing,[18–20] optical switching,[21,22] dispersion control,[23] slow light,[24,25] bandpass filtering,[26] and modulators.[27]

For the transmission spectrum of Fano resonance, the slope ratio (SR) and extinction ratio (ER) are two important parameters. Generally, having a high slope ratio (SR) and extinction ratio (ER) in the Fano spectrum is beneficial for applications, such as improving the sensitivity and response rate for sensors, optical switchers, and modulators. Based on Hybrid Electric (HE) mode components coupled whispering gallery mode, the Fano spectrum with a tunable SR can be realized by changing the coupling gap.[28] Based on Mach–Zehnder interferometers coupling with micro-ring resonators, high SR and ER can be realized.[17,29–31] Tunable SR means tunable line shape. One way to adjust the line shape of the transmission spectrum is to change the coupling gap,[8,12,28] another is thermo-optics tuning[9,11] or electric-optics tuning.[32] However, besides the systems to generate Fano resonance, these ways generally require additional large footprint devices to tune the line shape.

Here, a compact system without additional large footprint tunable devices to generate a Fano spectrum containing a Lorentz dip, a typical asymmetric shape, and an EIT-like peak at the same time was demonstrated. We propose a multimode interference model and experimentally demonstrate the interaction between two Fano resonance modes on thin film lithium niobite. The inverse design method was used to realize model fitting, validate our model, and analyze our model. Based on the parameters obtained by the inverse design, we further analyzed the influence of different parameters. Our research also shows that through the interaction of two Fano resonance modes, enhanced extinction ratio and tunable line shape can be realized in the transmission spectrum, which has potential applications in optical sensing.[33–36]

Figure 1(a) shows a coupling system consisting of a waveguide and micro-racetrack resonator. Light from the waveguide with a width of 0.8 μm is coupled to a micro-racetrack resonator with a width of 1 μm by pulley-coupling. The gap and the central angle are 0.6 μm and 30°. For the micro-racetrack resonator, the length of the straight part is L (90 μm) and the radius of the curved part is R (129 μm). The height of the device is 600 nm. Our device is fabricated on thin film

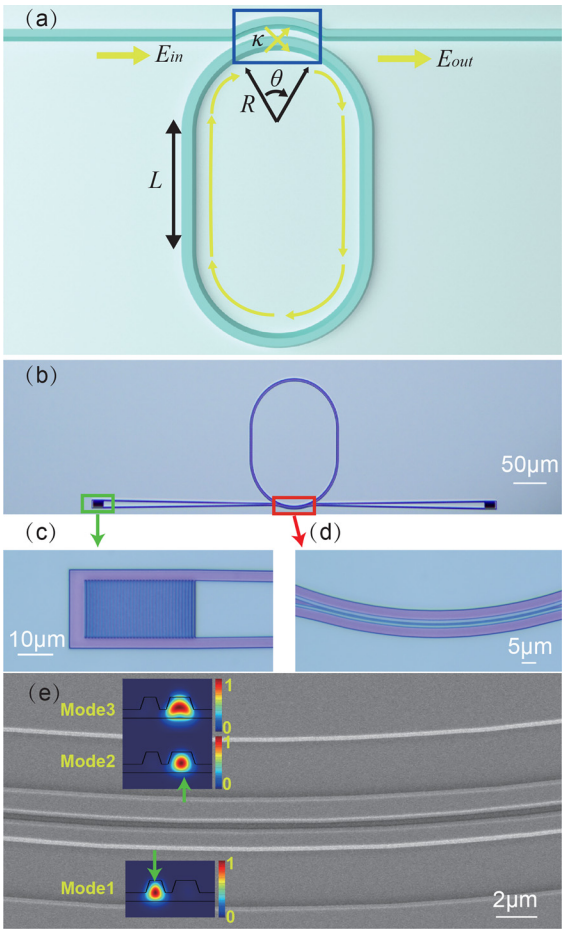

FIG. 1. Schematic illustration of coupling system and fabricated device. (a) Schematic illustration of coupling system consisting of the waveguide and micro-racetrack resonator. (b) Optical microscopic image of the fabricated device. (c) Grating coupler in (b) marked by a green rectangle. (d) Pulley-coupling region in (b) marked by a red rectangle. (e) Top view of the fabricated pulley-coupling region under a scanning electron microscope.

lithium niobate, and after etching, the tilt angle of the sidewall of the waveguide is about 60°. In the pulley-coupling region, considering the wavelength of input light is 1550 nm, there is only a TE_0 mode labeled as mode 1 in Fig. 1(e) in the waveguide with a width of 0.8 μm and there are two modes labeled as modes 2 and 3 in Fig. 1(e) allowed in the micro-racetrack with a width of 1 μm. So before going through the coupling region, the electric field in the waveguide with a width of 0.8 μm can be expressed as follows:

$$E_{in}(\omega) = a_1(\omega)e^{-i\varphi_1(\omega)}. \tag{1}$$

After going through the coupling region and propagating to the detector, the electric field in the waveguide without coupling to the micro-racetrack resonator can be expressed as follows:

$$E_2(\omega) = a_2(\omega)e^{-i\varphi_2(\omega)}. \tag{2}$$

Two modes of electric field are allowed in the micro-racetrack resonator. So for the light that is first coupled into, propagates in the micro-racetrack resonator, then coupled back to the waveguide and propagates to the detector, the electric field can be expressed as follows:

$$E_3(\omega) = a_3(\omega)e^{-i\varphi_3(\omega)}, \tag{3}$$

$$E_4(\omega) = a_4(\omega)e^{-i\varphi_4(\omega)}, \tag{4}$$

with

$$a_3(\omega) = \frac{-a_1\kappa_1^2\alpha_1}{e^{(i\varphi_{r_1}(\omega))} - t\alpha_1}, \quad a_4(\omega) = \frac{-a_1\kappa_2^2\alpha_2}{e^{(i\varphi_{r_2}(\omega))} - t\alpha_2}. \tag{5}$$

Here, $a_i(i = 1, 2, 3, 4)$ is the complex amplitude of the electric field E_i. $\alpha_i(i = 1, 2)$ is the amplitude transfer coefficient in a round trip propagation in the micro-racetrack resonator, and $\varphi_{r_i}(i = 1, 2)$ is the corresponding phase-shift determined by resonance. φ_1 is the initial phase of input light. $\varphi_i(i = 2, 3, 4)$ is the phase of output light due to coupling and propagation. $\kappa_i(i = 1, 2)$ is the coupling coefficient of $E_i(i = 3, 4)$. t is the transmission coefficient of E_{in}. Considering the energy conservation, $t^2 + \kappa_1^2 + \kappa_2^2 = 1$. So the total output electric field and transmission can be expressed as follows:

$$E_{out}(\omega) = E_2(\omega) + E_3(\omega) + E_4(\omega), \tag{6}$$

$$T(\omega) = \frac{|E_{out}(\omega)|^2}{|E_{in}(\omega)|^2}. \tag{7}$$

According to Eqs. (1)–(7), by giving different parameters, we can get the simulated results. However, there are many parameters in the theoretical model. It is not easy to adjust the parameters manually to get theoretical results that agree with the experimental results well. By inverse design, researchers can get the parameters of the desired devices according to their objective.[37–41] The process of inverse design can be summarized as follows: First, we start with the objects (device, model, or something else) that have different elements, and each element has tunable parameters x. Then we define the objective function $f(x)$, the objective function can be transmission or something else. Then, during the simulation, we use a specific algorithm to maximize or minimize the objective function. Finally, we end up with optimized parameters to maximize or minimize the objective function. The inverse design method is not only an effective way to design the photonic device but also can be useful for proving the theoretical model. Here, the inverse design method was used to realize model fitting, validate our model, and analyze our model. Two different algorithms were used to prove our theoretical model, respectively. During the inverse design, the objective function $f(x)$ was set as follows:

$$f(x) = \min \sum_i^n |T_{sim}^{\omega(i)} - T_{exp}^{\omega(i)}|^2, \tag{8}$$

where $\omega(i)$ is the ith frequency, $T_{sim}^{\omega(i)}$ is the simulated transmission at frequency of $\omega(i)$ according to Eq. (7), $T_{exp}^{\omega(i)}$ is the experimental transmission at frequency of $\omega(i)$.

Figure 1(b) shows the top-view optical image of the fabricated device consisting of a grating coupler, waveguide taper, and micro-racetrack resonator. The whole device is fabricated on thin film lithium niobite by standard electron beam lithography and reactive ion etching. Details of the fabrication process can be found in our previous work.[42] Figure 1(c) shows the grating coupler in Fig. 1(b) marked by a green

rectangle. Here, the grating coupler has a period of 900 nm and a duty ratio of 0.35. Figure 1(d) shows the pulley-coupling region in Fig. 1(b) marked by a red rectangle. Figure 1(e) shows the top view of the fabricated pulley-coupling region under a scanning electron microscope.

Light from a tunable laser is coupled into the X-cut thin film lithium niobite with a thickness of 600 nm and an etching depth of 0.35 μm by grating coupler, then goes through an adiabatic waveguide taper with a width decreased from 15 to 0.8 μm and a length of 450 μm, then goes through a waveguide with a width of 0.8 μm. Output light was collected by a photodetector and then shown on the oscilloscope. The transmission spectrum was measured and then normalized to the maximum value as shown in Fig. 2. In the transmission spectrum, the resonance line shape varies from the wavelength and almost all the line shapes are close to the Fano line shape. To further investigate the spectrum, Eq. (9) is used to fit these resonance line shapes, which is a common Fano function,[43]

$$T = T_0 + \frac{A\left(q + 2\frac{\lambda - \lambda_0}{w}\right)^2}{1 + \left(2\frac{\lambda - \lambda_0}{w}\right)^2}, \tag{9}$$

where T is the transmission, T_0 is the background intensity, w is the loss-related linewidth, q is the Fano factor that characterizes the asymmetry degree of the line shape, λ_0 is the resonance wavelength, and A is an amplitude coefficient. Different line shapes were chosen for the university, and simulated results in Figs. 3(a) and 3(b) both have a great agreement with the experimental results, exhibiting these resonance line shapes are Fano line shapes. The fitting values for q and λ_0 are −64.96 and 1543.3 in Fig. 3(a) and the fitting values for q and λ_0 are 37.16 and 1543.5 in Fig. 3(b). The line shape of the spectrum changes with the wavelength from 1523 to 1550 nm in Fig. 2. In Fig. 2, the line shape changes from a Lorentz dip to a typical asymmetric shape when the wavelength of light changes from 1523 to 1540 nm. When the wavelength of light changes from 1540 to 1550 nm, an EIT-like peak appears. It shows the capability of tuning the line shape from one type to another by selecting the specific wavelength. So here

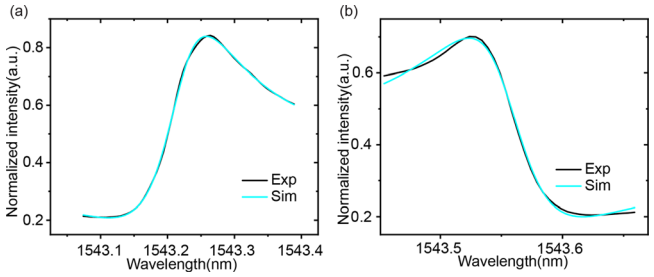

FIG. 3. Demonstration of the Fano line shapes. (a) and (b) Experimental data and fitting data according to the common Fano function around 1543.3 nm/1543.5 nm.

we show the wide-range tunable line shape based on the interaction of two Fano resonance modes. In Fig. 2, the free spectrum range (FSR) of peaks marked in red is smaller than the free spectrum range (FSR) of peaks marked in green. And the FSR around eigenfrequency ω can be approximated as $FSR = c/n_g R$, where n_g is the group index around ω and R is the radius of the micro-cavity. Here, based on simulation, the n_g around 1545 nm of mode 2 is 2.387 smaller than the n_g around 1545 nm of mode 3, which is 2.394. So the FSR of mode 2 is larger than the FSR of mode 3. So the peaks marked in red are due to the interference of modes 1 and 3, and the peaks marked in green are due to the interference of modes 1 and 2.

To show the results of model fitting and verify our theoretical model, Fig. 4 shows the comparison between the experimental results and theoretical results around 1525, 1533, and 1545 nm, respectively. The simulated results in Fig. 4 were obtained by inverse design and the algorithms used during the inverse design are the butterfly optimization algorithm (BOA) and the particle swarm optimization (PSO), respectively. The algorithms run on an office computer with a CPU of Intel Core i5-7500 and with a RAM of 16 GB. The theoretical results obtained by inverse design have a great agreement with the experiment results. Detailed parameters corresponding Fig. 4 are shown in Table I. $\Delta\varphi_{32}(\omega)$ is the phase difference between $\varphi_3(\omega)$ and $\varphi_2(\omega)$, and $\Delta\varphi_{42}(\omega)$ is the phase difference between $\varphi_4(\omega)$ and $\varphi_2(\omega)$. By

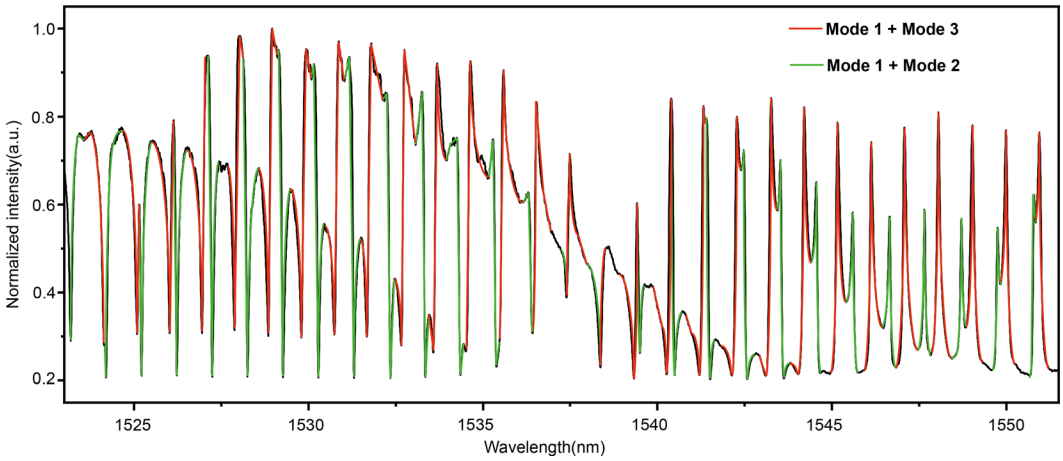

FIG. 2. Transmission spectrum of the device. The peaks marked in red are due to the interference of modes 1 and 3 and the peaks marked in green are due to the interference of modes 1 and 2.

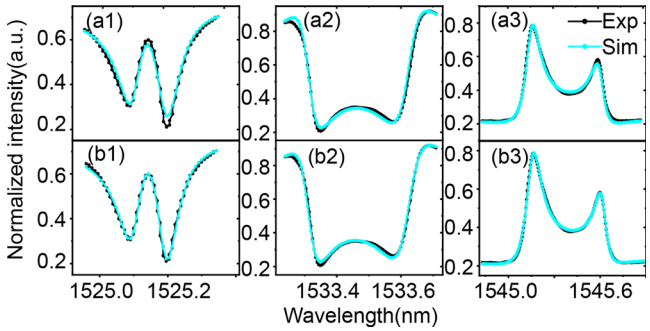

FIG. 4. Comparison between the experimental results and theoretical results. (a1)–(a3) Theoretical results obtained by BOA and experimental results. (b1)–(b3) Theoretical results obtained by PSO and experimental results.

analyzing the simulated results in Table I, α_1, α_2, hardly change with wavelength, which means the loss of light with different wavelengths in the micro-racetrack resonator is similar. t decreases slowly with increasing wavelength due to the different coupling coefficients of different wavelengths. $(1-t^2)/\kappa_1^2$ is the ratio of the energy of mode 2 to the total energy coupled into the cavity. φ_2 decreases slowly with increasing wavelength due to the coupling and dispersion. Only $\Delta\varphi_{32}(\omega)$ and $\Delta\varphi_{42}(\omega)$ change a lot with wavelength, which means the line shapes are different with wavelength, mainly due to the different phase differences between mode 1 in the waveguide and modes 2 and 3 in the micro-racetrack resonator. During the inverse design, the results obtained by different algorithms were a little different. Among the two algorithms, the best value of the objective function is obtained by PSO. Figures 4(b1)–4(b3) show a better match between experimental results and simulated results than Figs. 4(a1)–4(a3).

Further investigating the spectrum, we found that the interaction between two Fano resonance modes can influence the extinction ratio (ER) of the Fano line shapes, which is shown in Fig. 5. Based on Fig. 2, we find there is only one obvious Fano resonance mode due to the interference of modes 1 and 3 in Fig. 5 indicating the weak interaction of two Fano resonance modes, while there are two obvious Fano resonance modes in Fig. 5(b), indicating the strong interaction of two Fano resonance modes. The ER in Fig. 5(b) is more than 1.5 times larger than the ER in Fig. 5(a), which shows the strong interaction between two Fano resonance modes can improve the ER. The enhanced ER is due to the interference of two modes. This characteristic shows the potential applications in optical sensing.

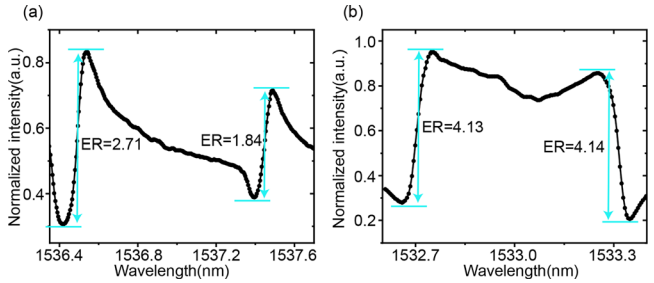

FIG. 5. Extinction ratio (ER) around different wavelengths. (a) and (b) Extinction ratio (ER) around 1537/1533 nm.

We acknowledge the Center for Advanced Electronic Materials and Devices (AEMD) of the Shanghai Jiao Tong University for the fabrication support. We acknowledge support from the National Natural Science Foundation of China (Grant No. 12134009) and the Shanghai Jiao Tong University (SJTU) (Grant No. 21X010200828).

AUTHOR DECLARATIONS

Conflict of Interest

The authors have no conflicts to disclose.

Author Contributions

Zhiwei Wei and Tingge Yuan contributed equally to this work.

Zhiwei Wei: Investigation (lead); Methodology (lead); Validation (lead); Writing – original draft (lead); Writing – review & editing (lead). **Tingge Yuan:** Data curation (equal); Methodology (equal); Writing – review & editing (equal). **Jiangwei Wu:** Validation (supporting). **Chengyu Chen:** Validation (supporting). **Yuping Chen:** Funding acquisition (lead); Writing – review & editing (supporting). **Xianfeng Chen:** Funding acquisition (equal).

DATA AVAILABILITY

The data that support the findings of this study are available on request from the corresponding author. The data are not publicly available due to state restrictions such as privacy or ethical restrictions.

TABLE I. Parameters obtained by inverse design.

λ (nm)	α_1	α_2	t	$(1-t^2)/\kappa_1^2$	$\varphi_2(\pi)$	$\Delta\varphi_{32}(\pi)$	$\Delta\varphi_{42}(\pi)$	Algorithm
1525	0.979	0.979	0.983	0.45	0.25	1.76	1.40	BOA
1533	0.973	0.988	0.979	0.53	0.20	1.96	1.27	
1545	0.982	0.986	0.970	0.43	0.06	1.23	0.63	
1525	0.983	0.976	0.984	0.52	0.22	2.00	1.62	PSO
1533	0.988	0.975	0.981	0.41	0.20	1.95	1.25	
1545	0.992	0.984	0.970	0.35	0.14	1.03	0.47	

REFERENCES

[1]M. F. Limonov, M. V. Rybin, A. N. Poddubny, and Y. S. Kivshar, Nat. Photonics **11**, 543 (2017).
[2]Y.-C. Liu, B.-B. Li, and Y.-F. Xiao, Nanophotonics **6**, 789 (2017).
[3]Y. Shuai, D. Zhao, A. Singh Chadha, J.-H. Seo, H. Yang, S. Fan, Z. Ma, and W. Zhou, Appl. Phys. Lett. **103**, 241106 (2013).
[4]H. Lu, X. Liu, D. Mao, and G. Wang, Opt. Lett. **37**, 3780 (2012).
[5]B. Luk'yanchuk, N. I. Zheludev, S. A. Maier, N. J. Halas, P. Nordlander, H. Giessen, and C. T. Chong, Nat. Mater. **9**, 707 (2010).
[6]C.-H. Dong, C.-L. Zou, Y.-F. Xiao, J.-M. Cui, Z.-F. Han, and G.-C. Guo, J. Phys. B **42**, 215401 (2009).
[7]B.-B. Li, Y.-F. Xiao, C.-L. Zou, Y.-C. Liu, X.-F. Jiang, Y.-L. Chen, Y. Li, and Q. Gong, Appl. Phys. Lett. **98**, 021116 (2011).
[8]Y. Yang, S. Saurabh, J. Ward, and S. N. Chormaic, Opt. Lett. **40**, 1834 (2015).
[9]T. Hu, P. Yu, C. Qiu, H. Qiu, F. Wang, M. Yang, X. Jiang, H. Yu, and J. Yang, Appl. Phys. Lett. **102**, 011112 (2013).
[10]Q. Huang, Z. Shu, G. Song, J. Chen, J. Xia, and J. Yu, Opt. Express **22**, 3219 (2014).
[11]L. Zhou, B. Wang, S. Zheng, and W. Zhang, IEEE Photonics J. **14**, 6641105 (2022).
[12]Y.-L. Shang, M.-Y. Ye, and X.-M. Lin, Photonics Res. **5**, 119 (2017).
[13]B.-B. Li, Y.-F. Xiao, C.-L. Zou, X.-F. Jiang, Y.-C. Liu, F.-W. Sun, Y. Li, and Q. Gong, Appl. Phys. Lett. **100**, 021108 (2012).
[14]S. Yuan, L. Chen, Z. Wang, R. Wang, X. Wu, and X. Zhang, Appl. Phys. Lett. **115**, 201102 (2019).
[15]L. Y. M. Tobing, D. Lim, P. Dumon, R. Baets, and M.-K. Chin, Appl. Phys. Lett. **92**, 101122 (2008).
[16]C. Qiu, P. Yu, T. Hu, F. Wang, X. Jiang, and J. Yang, Appl. Phys. Lett. **101**, 021110 (2012).
[17]Y. Xu, L. Lu, G. Chen, J. Liao, X. Xu, J. Ou, and L. Zhu, Photonics **9**, 725 (2022).
[18]Y. Zhang, Y.-R. Zhen, O. Neumann, J. K. Day, P. Nordlander, and N. J. Halas, Nat. Commun. **5**, 4424 (2014).
[19]W. Lin, H. Zhang, S.-C. Chen, B. Liu, and Y.-G. Liu, Opt. Express **25**, 994 (2017).
[20]J. Wang, X. Zhang, M. Yan, L. Yang, F. Hou, W. Sun, X. Zhang, L. Yuan, H. Xiao, and T. Wang, Photonics Res. **6**, 1124 (2018).
[21]J.-H. Wu, J.-Y. Gao, J.-H. Xu, L. Silvestri, M. Artoni, G. C. La Rocca, and F. Bassani, Phys. Rev. Lett. **95**, 057401 (2005).
[22]L. Stern, M. Grajower, and U. Levy, Nat. Commun. **5**, 4865 (2014).
[23]M. F. Limonov, Adv. Opt. Photonics **13**, 703 (2021).
[24]Q. Xu, P. Dong, and M. Lipson, Nat. Phys. **3**, 406 (2007).
[25]K. Totsuka, N. Kobayashi, and M. Tomita, Phys. Rev. Lett. **98**, 213904 (2007).
[26]H. Wang, R. Xu, J. Zhang, W. Zhou, and D. Shen, Opt. Express **27**, 22717 (2019).
[27]W. Zhao, H. Jiang, B. Liu, Y. Jiang, C. Tang, and J. Li, Appl. Phys. Lett. **107**, 171109 (2015).
[28]X. Gan, Z. Ban, F. Gao, F. Bo, G. Zhang, and J. Xu, J. Lightwave Technol. **41**, 2501 (2023).
[29]A. Li and W. Bogaerts, APL Photonics **2**, 096101 (2017).
[30]S. Liao, T. Zhang, H. Bao, Y. Liu, and L. Liu, IEEE Photonics J. **14**, 7809908 (2022).
[31]X. Liu, Y. Yu, and X. Zhang, Opt. Lett. **44**, 251 (2019).
[32]S. Darmawan, L. Y. M. Tobing, and T. Mei, Opt. Lett. **35**, 238 (2010).
[33]X. Wang, J. Wu, C. Chen, T. Yuan, Y. Chen, and X. Chen, Appl. Phys. Lett. **124**, 061108 (2024).
[34]X. Wang, T. Yuan, J. Wu, Y. Chen, and X. Chen, Laser Photonics Rev. **18**, 2300760 (2024).
[35]S. Farhadi, M. Miri, and A. Farmani, J. Opt. Soc. Am. B **40**, 2723 (2023).
[36]F. Wu, J. Wu, Z. Guo, H. Jiang, Y. Sun, Y. Li, J. Ren, and H. Chen, Phys. Rev. Appl. **12**, 014028 (2019).
[37]X. He, D. Sun, J. Chen, and Y. Shi, IEEE Photonics J. **16**, 6600305 (2024).
[38]J. Lyu, T. Zhu, Y. Zhou, Z. Chen, Y. Pi, Z. Liu, X. Xu, K. Xu, X. Ma, L. Wang *et al.*, Opto-Electron. Sci. **2**, 230038 (2023).
[39]R. Shen, B. Hong, X. Ren, F. Yang, W. Chu, H. Cai, and W. Huang, J. Nanophotonics **18**, 010901 (2024).
[40]C. Shang, J. Yang, A. M. Hammond, Z. Chen, M. Chen, Z. Lin, S. G. Johnson, and C. Wang, ACS Photonics **10**, 1019 (2023).
[41]S. Molesky, Z. Lin, A. Y. Piggott, W. Jin, J. Vucković, and A. W. Rodriguez, Nat. Photonics **12**, 659 (2018).
[42]T. Yuan, J. Wu, Y. Liu, X. Yan, H. Jiang, H. Li, Z. Liang, Q. Lin, Y. Chen, and X. Chen, Sci. China: Phys., Mech. Astron. **66**, 284211 (2023).
[43]T. Yuan, X. Wang, J. Wu, H. Li, Y. Chen, and X. Chen, Laser Photonics Rev. 2400457 (2024).